

Human3R: Incorporating Human Priors for Better 3D Dynamic Reconstruction from Monocular Videos

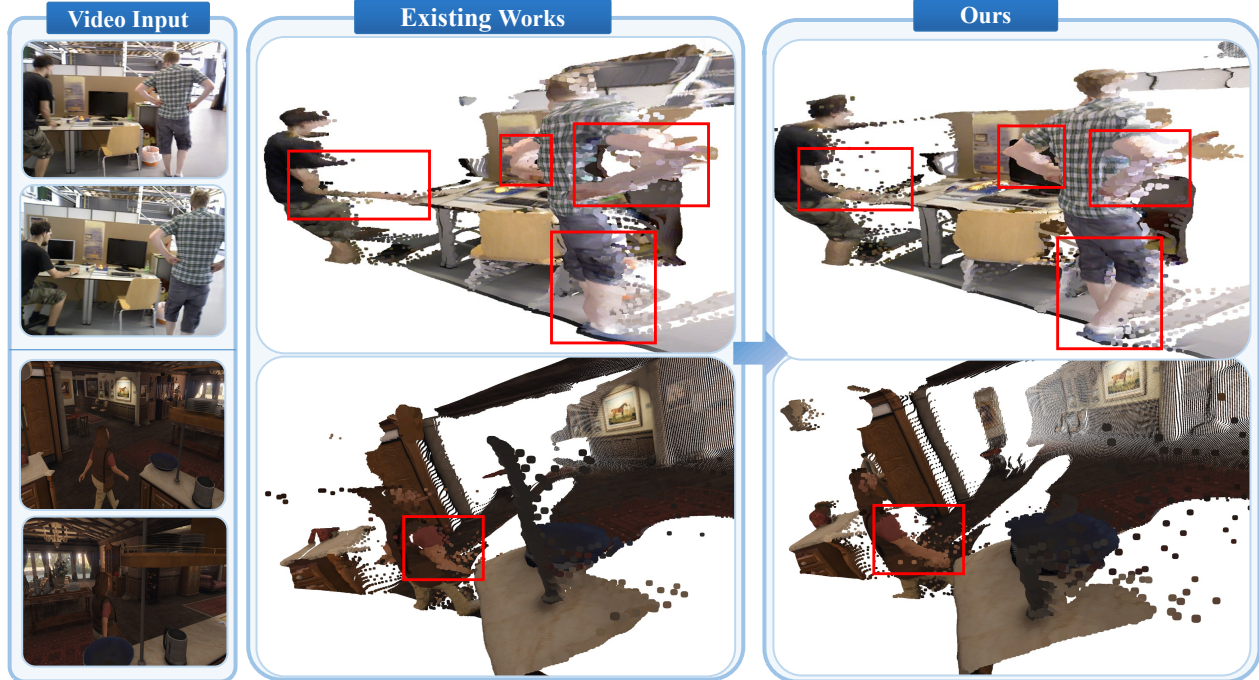
Weitao Xiong^{1,2*}Zhiyuan Yuan^{3*}Jiahao Lu¹Chengfeng Zhao¹Peng Li¹Yuan Liu^{1†}¹HKUST²XMU³SYSU

Figure 1. **Human3R for Dynamic Scene Reconstruction.** Our task is to reconstruct accurate 3D point clouds from monocular videos containing humans. By incorporating SMPL human priors, Human3R achieves superior reconstruction quality for both dynamic human motions and static scene elements compared to existing methods. The highlighted regions demonstrate our method’s ability to preserve anatomically consistent human geometry and fine-grained details while maintaining overall scene coherence.

Abstract

Monocular dynamic video reconstruction faces significant challenges in dynamic human scenes due to geometric inconsistencies and resolution degradation issues. Existing methods lack 3D human structural understanding, producing geometrically inconsistent results with distorted limb proportions and unnatural human-object fusion, while memory-

constrained downsampling causes human boundary drift toward background geometry. To address these limitations, we propose to incorporate hybrid geometric priors that combine SMPL human body models with monocular depth estimation. Our approach leverages structured human priors to maintain surface consistency while capturing fine-grained geometric details in human regions. We introduce Human3R, featuring a hierarchical pipeline with refinement components that processes full-resolution images for overall scene geometry, then applies strategic cropping and cross-attention fusion for human-specific detail enhancement. The method integrates

*Equal contribution.

†Corresponding author.

SMPL priors through a Feature Fusion Module to ensure geometrically plausible reconstruction while preserving fine-grained human boundaries. Extensive experiments on TUM Dynamics and GTA-IM datasets demonstrate superior performance in dynamic human reconstruction.

1. Introduction

Recovering both camera motion and geometry from monocular dynamic video is still a challenging task in computer vision, with applications ranging from robotics to augmented reality. Traditional methods utilize Structure-from-Motion (SfM), which involve iterative optimization techniques, such as Bundle Adjustment (BA), to recover the static scene structure. However, these methods are limited by their reliance on feature correspondences, which are often sparse. Recent methods [43] address this problem in a data-driven manner, where DUS3R [43] bypasses the need for explicit feature matching by directly learning scene geometry and motion from image pair input, enabling faster, more accurate, and more robust handling of the dense 3D geometry. However, they are specifically designed for static scenes, which cannot be directly generalized to monocular dynamic video input.

Prior works have proposed several methods for handling dynamic scenes. MonST3R [51] fine-tunes the DUS3R model on dynamic data and introduces a new optimization method specifically designed for dynamic scenes. Align3R [33] enhances DUS3R [43] by incorporating a depth prior, improving its performance on monocular dynamic video input. Meanwhile, Easi3R [10] extends DUS3R to dynamic environments by disentangling attention maps to separate dynamic and static motion. VGGT [41] addresses this challenge by jointly training a large transformer on both static and dynamic data, allowing for better generalization across diverse scenarios.

While these methods demonstrate strong performance on general dynamic scenes, they still have two issues in the domain of precise human depth estimation. 1. *Anatomical Artifacts*: Due to the lack of adequate 3D human structural understanding, existing methods often produce geometrically inconsistent results—such as distorted limb proportions, disconnected body parts, and unnatural human-object fusion. 2. *Resolution and Boundary Degradation*: Humans typically occupy small pixel regions in scene images, and memory-constrained image downsampling (from 1080×1920 to 288×512) exacerbates this issue by causing ViT tokenization tends to blend foreground human and background information within the same spatial tokens. Consequently, reconstructed human boundaries drift toward background geometry, losing fine-grained human details.

To address the aforementioned challenges, we propose a novel method, **Human3R**. To mitigate the Anatomical Artifacts issue, we introduce a hybrid geometric prior that com-

bines the Skinned Multi-Person Linear (SMPL) model with monocular depth estimation. Specifically, the SMPL model provides a consistent human surface prior, while monocular depth estimation contributes fine-grained geometric details. By aligning the SMPL geometry with the monocular depth map, we obtain detailed depth predictions that maintain strong surface consistency. Furthermore, to tackle the Resolution and Boundary Degradation issue, we design a pipeline with a refinement component. The network initially processes the full-resolution image to capture the overall scene geometry. When humans appear small in the image, our refinement module applies strategic image cropping to effectively super-resolve human regions. A dedicated branch then employs cross-attention between the enlarged human region and the original image context, enabling precise reconstruction of human-like forms and ultimately producing more detailed and accurate human reconstruction results.

Our main contributions are summarized as follows:

- We propose a novel model, **Human3R**, capable of accurate dynamic human reconstruction.
- To address the Anatomical Artifacts issue, we incorporate a hybrid geometric prior that combines the SMPL model with monocular depth, enabling detailed depth prediction while maintaining strong surface consistency.
- To mitigate the Resolution and Boundary Degradation issue, we design a hierarchical pipeline with a refinement component: the network initially processes full-resolution images to capture overall scene geometry, then applies a dedicated cropping mechanism and cross-attention fusion to refine human-specific details when humans appear small in the scene.
- Extensive experiments demonstrate the effectiveness of our approach, with results on the **TUM dynamics** and **GTA-IM** datasets validating its strong performance in dynamic human reconstruction.

2. Related Work

Feed-Forward 3D Reconstruction Recent advancements in feed-forward 3D reconstruction [5, 7, 14, 22, 27, 31, 34, 39, 40, 43] have focused on directly regressing dense scene geometry from image inputs without relying on iterative optimization. DUS3R [43] introduces a dense and unconstrained stereo reconstruction framework that predicts local pointmaps from image pairs without known camera poses or calibration, achieving global consistency via lightweight alignment. Recent extensions such as [5, 14, 39, 40] eliminate DUS3R’s dependence on global optimization. While these approaches offer efficient and accurate reconstruction of static environments, they are not designed for dynamic scenes, particularly those containing human subjects.

Feed-Forward 4D Reconstruction Recent feed-forward 4D reconstruction methods aim to recover time-varying

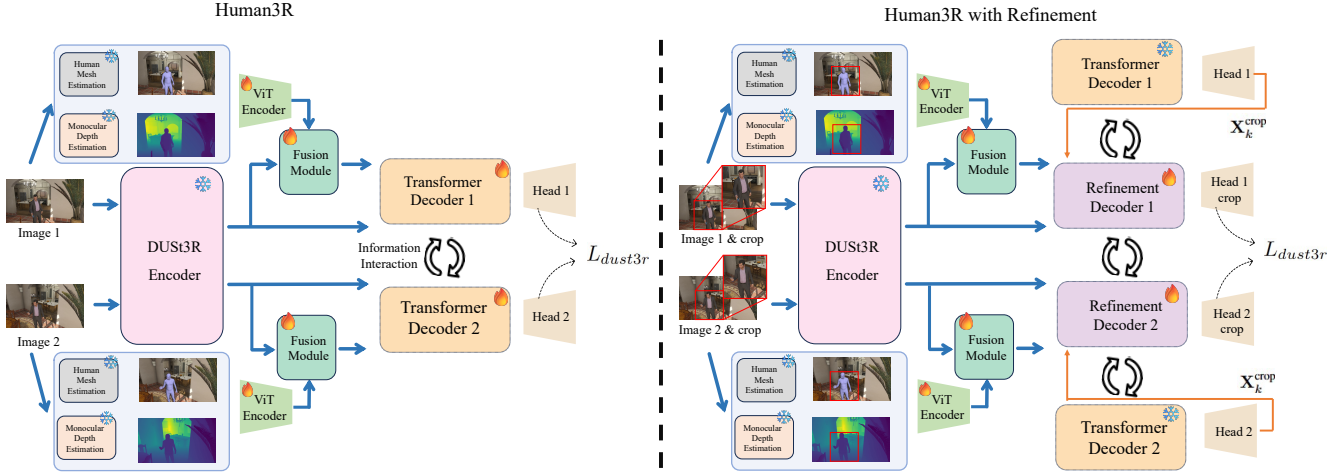


Figure 2. **The overview of our framework.** The left shows the base Human3R pipeline that processes image pairs through DUS3R encoders, followed by a Feature Fusion Module that integrates image features, monocular depth features, and SMPL depth features via cross-attention mechanism and gated operations. The fused features are then processed through transformer decoders to produce initial point map reconstruction. The right illustrates Human3R with Refinement, which is activated when humans occupy small pixel regions in the input images. The refinement stage crops human regions from the input images, upsamples the point clouds, and processes them through refinement decoders that incorporate cross-module attention between local crop features and preserved scene context. This hierarchical design enables high-fidelity human reconstruction while maintaining geometric consistency between human regions and the surrounding scene.

scene geometry from monocular dynamic video [7]. MonST3R [51] extends DUS3R by introducing temporal consistency losses and re-optimization strategies to better capture dynamic motion. CUT3R [42] addresses dynamic reconstruction by using a stateful recurrent transformer to accumulate 3D information across frames into a persistent spatial memory, enabling online and globally aligned 4D reconstruction. Easi3R [10] improves generalization to deformable objects by disentangling appearance and motion via attention mechanisms. VGGT [12, 41, 44] and Rig3R [26] trains large transformer models jointly on static and dynamic datasets to enhance overall robustness. Uni4D [48] introduces a multi-stage optimization framework that harnesses multiple pretrained models to advance dynamic 3D modeling. Geo4D [23] repurposes video diffusion models to predict multi-modal geometric outputs—point, depth, and ray maps—and fuses them at test time for accurate long-range dynamic scene reconstruction. GeometryCrafter [46], on the other hand, uses a point-map VAE and diffusion-based sequence modeling to estimate high-fidelity, temporally coherent point map sequences from real-world videos. Among these, Align3R [33] offers a simple yet effective strategy by injecting depth prior into DUS3R’s pointmap framework, improving details and temporal consistency in dynamic environments. However, these methods treat human regions as unstructured geometry and overlook the blended information between the foreground and background, often leading to anatomical artifacts and boundary degradation. MegaSAM [28] and VIPE [21] combine the advantages of feed forward model and post-alignment tech-

niques, demonstrating impressive results. Others method like [9, 11, 12, 16, 20, 29, 41, 45, 50, 52] utilize 2D/3D tracks or motion prediction [30] to improve the reconstruction quality. In contrast, our method builds upon Align3R, incorporating a hybrid geometric prior and proposing a refinement strategy to achieve anatomically coherent and address the boundary degradation.

Monocular Depth Estimation Monocular depth estimation methods such as MiDaS [37], DepthAnything [47], and DepthPro [4] have demonstrated strong performance in producing accurate single-image depth maps through large-scale training on both labeled and unlabeled data. MiDaS [37] mixes diverse datasets to achieve robust zero-shot generalization across domains, while DepthAnything [47] scales up to millions of unlabeled images for improved robustness. DepthPro [4] further incorporates metric-scale supervision and sharp-detail modeling for precise depth predictions. Additional works [1, 15, 17, 18, 37] explore directions such as improved zero-shot transfer, dense transformer architectures, adaptive binning, autoregressive refinement, and enhanced robustness under challenging conditions. While monocular depth estimation generally provides detailed and high-quality geometric cues, it is inherently frame-independent and thus prone to temporal inconsistency and flickering when applied to video sequences—issues that are especially pronounced in dynamic scenes involving humans. Moreover, monocular depth methods often produce degraded predictions on human surfaces, leading to anatomical artifacts such as distorted limbs, inconsistent body contours, and missing fine-scale geometry. These challenges motivate the need for approaches

that preserve detailed geometry, ensure surface consistency, and maintain temporal stability in dynamic human reconstruction.

Human Mesh Estimation and Recovery Recent human mesh recovery approaches [13, 19, 24, 25, 49] have made significant progress by leveraging strong backbones and large-scale 3D datasets. Most of these methods, including HMR [24], SPIN [25], and HMR2.0 [19], adopt a weak-perspective camera model to simplify training, which however leads to scale ambiguity in real-world scenes. More recent works such as TokenHMR [13] and GLAMR [49] highlight the importance of accurate camera modeling and spatiotemporal consistency, yet still suffer from misalignment when projecting 3D poses into image space. CameraHMR [36] addresses this issue by learning full-perspective camera parameters during training and inference, significantly improving scale stability and geometric alignment. Given that our method relies on accurate depth priors and consistent human geometry across frames, we adopt CameraHMR to obtain reliable SMPL estimates under dynamic camera motions.

3. Method

3.1. Overview

Given a video consisting of N frames $\{\mathbf{I}_k \in \mathbb{R}^{H \times W \times 3}\}_{k=1}^N$, our target is to estimate the corresponding depth maps $\{\mathbf{D}_k \in \mathbb{R}^{H \times W}\}_{k=1}^N$ and camera poses $\{\pi_k \in \text{SE}(3)\}_{k=1}^N$. Human3R achieves this through a hierarchical pipeline with a refinement:

- **Global Scene Processing.** We estimate coarse depth maps for all frames and generate global point clouds by fusing monocular cues with parametric human priors via a feature fusion module.
- **Human-Centric Refinement.** When humans appear small in the scene, we crop both the input images and the initial point clouds to the localized human regions. A dedicated network branch then performs cross-attention between the enlarged human region and the original image context. This design facilitates more accurate point cloud alignment and subsequent refinement, ensuring proper human-like form reconstruction.

3.2. Global Scene Processing

3.2.1 Aligning Depth with SMPL Priors

To ensure consistent depth representation across different estimation sources, we align the monocular depth maps $\{\hat{\mathbf{D}}_k^{\text{Mono}}\}_{k=1}^N$ with the SMPL depth maps $\{\hat{\mathbf{D}}_k^{\text{SMPL}}\}_{k=1}^N$ via a robust linear fitting scheme based on RANSAC. For each frame k , a binary human mask $\mathbf{M}_k \in \{0, 1\}^{H \times W}$ is obtained from the 2D SMPL pose to define valid human regions. Given a monocular depth map $\hat{\mathbf{D}}_k^{\text{Mono}}$, only the depth

values inside the valid mask are extracted to exclude background pixels. Let $\mathbf{d}_{\text{mono}} \in \mathbb{R}^n$ and $\mathbf{d}_{\text{smpl}} \in \mathbb{R}^n$ denote the flattened depth vectors from $\hat{\mathbf{D}}_k^{\text{Mono}}$ and $\hat{\mathbf{D}}_k^{\text{SMPL}}$, respectively, at the n valid pixel locations. RANSAC is then applied to estimate the scale factor s and offset b of the optimal linear transformation:

$$\mathbf{d}_{\text{smpl}}(i) \approx s \cdot \mathbf{d}_{\text{mono}}(i) + b, \quad i = 1, \dots, n, \quad (1)$$

where $\mathbf{d}_{\text{smpl}}(i)$ and $\mathbf{d}_{\text{mono}}(i)$ are the depth values at the i -th valid pixel. The RANSAC algorithm proceeds by iteratively sampling random subsets of two points from \mathbf{d}_{mono} and \mathbf{d}_{smpl} , fitting a linear model, and evaluating the number of inliers within a predefined residual threshold τ (set to 0.001 in our implementation). The model with the highest number of inliers after a fixed number of iterations (e.g., 1000) is selected, yielding the best scale s^* and shift b^* .

Finally, the aligned monocular depth map $\hat{\mathbf{D}}_k^{\text{Aligned}}$ is obtained by applying the transformation to the entire $\hat{\mathbf{D}}_k^{\text{Mono}}$ as follows:

$$\hat{\mathbf{D}}_k^{\text{Aligned}}(x, y) = s^* \cdot \hat{\mathbf{D}}_k^{\text{Mono}}(x, y) + b^*, \quad (2)$$

for all pixel coordinates (x, y) . Additionally, we leverage the focal length predicted by the Human Mesh Estimation model for the SMPL representation as a reference in point map reconstruction. The aligned depth map, $\hat{\mathbf{D}}_k^{\text{Aligned}}$, and the SMPL depth map, $\hat{\mathbf{D}}_k^{\text{SMPL}}$, are subsequently unprojected into point maps, $\hat{\mathbf{X}}_k^{\text{Aligned}}$ and $\hat{\mathbf{X}}_k^{\text{SMPL}}$, using the SMPL focal length.

3.2.2 Feature Fusion Module

After obtaining the point maps from the aligned monocular depth map $\hat{\mathbf{D}}_k^{\text{Aligned}}$ and the SMPL depth map $\hat{\mathbf{D}}_k^{\text{SMPL}}$, we aim to fuse their geometric and contextual information to enhance the representation of the human body in 3D space. To achieve this, we employ a cross-attention mechanism to integrate features extracted from both point maps, followed by a gated operation to adaptively control the contribution of the fused features. This Feature Fusion Module is applied before the decoder in both Stage 1 and Stage 2 of our pipeline.

Point map ViT. We first extract point map features $\hat{\mathbf{F}}_{\text{mono}}$ and $\hat{\mathbf{F}}_{\text{smpl}}$ using trainable lightweight ViT-based encoders. To process the point maps, we apply a patch embedding method to divide the input point maps into patches and embed them into feature tokens, formulated as:

$$\hat{\mathbf{F}}_i = \text{PatchEmbed}(\hat{\mathbf{X}}_i), \quad (3)$$

where $\hat{\mathbf{X}}_i$ represents the input point map, and $\hat{\mathbf{F}}_i$ is the corresponding patchified feature representation with shape dependent on the patch size and embedding dimension.

Cross Attention Module. To maintain DUST3R’s robust feature extraction capabilities, the image encoder is frozen. image features $\hat{\mathbf{F}}_{\text{img}}$ are extracted from the input views using this frozen ViT encoder. A cross-attention module is then applied to integrate above features. Specifically, the query is formed by concatenating $\hat{\mathbf{F}}_{\text{img}}$ and $\hat{\mathbf{F}}_{\text{mono}}$ followed by a linear projection, while $\hat{\mathbf{F}}_{\text{smp}}$ serves as both the key and value after a separate projection. This mechanism allows the module to attend to relevant geometric cues in the SMPL depth features, producing an output feature set $\hat{\mathbf{F}}_{\text{cross}}$ that captures interdependencies among the image, monocular depth, and SMPL depth features. The cross-attention output is computed as:

$$\hat{\mathbf{F}}_{\text{cross}} = \text{MultiAtten}(\mathbf{Q}(\hat{\mathbf{F}}_{\text{img}}, \hat{\mathbf{F}}_{\text{mono}}), \mathbf{K}(\hat{\mathbf{F}}_{\text{smp}}), \mathbf{V}(\hat{\mathbf{F}}_{\text{smp}})), \quad (4)$$

where $\mathbf{Q}(\cdot)$, $\mathbf{K}(\cdot)$, and $\mathbf{V}(\cdot)$ denote the respective projections, and $\text{Multi-Atten}(\cdot)$ represents the multi-head attention mechanism.

Gate Mechanism. To adaptively integrate $\hat{\mathbf{F}}_{\text{cross}}$ with the original monocular features $\hat{\mathbf{F}}_{\text{mono}}$, we use a gate mechanism to compute a gate \mathbf{G} , which determines the contribution of $\hat{\mathbf{F}}_{\text{cross}}$. The gate is derived from the concatenation of $\hat{\mathbf{F}}_{\text{cross}}$, $\hat{\mathbf{F}}_{\text{mono}}$, and $\hat{\mathbf{F}}_{\text{smp}}$ through a series of linear transformations and activations. The final fused feature is obtained as:

$$\hat{\mathbf{F}}_{\text{fused}} = \hat{\mathbf{F}}_{\text{mono}} + \mathbf{G} \odot \hat{\mathbf{F}}_{\text{cross}}, \quad (5)$$

where \odot denotes element-wise multiplication. This gated integration ensures that the cross-attention features selectively enhance the original monocular features, preserving critical geometric information while incorporating complementary cues from the SMPL depth map.

3.2.3 Decoder Module

We process the full scene images $\{\mathbf{I}_k\}_{k=1}^N$ to establish global context. The fused features $\hat{\mathbf{F}}_{\text{fused}}$ from the Feature Fusion Module are processed through self-attention to generate multi-level features $\hat{\mathbf{F}}_{\text{fused}}^{(1)}, \hat{\mathbf{F}}_{\text{fused}}^{(2)}, \dots, \hat{\mathbf{F}}_{\text{fused}}^{(s)}$, which are injected into the DUST3R decoder via zero convolution:

$$\hat{\mathbf{E}}_{\text{scene}}^{(l)} = \text{ZeroConv}(\hat{\mathbf{F}}_{\text{fused}}^{(l)}) + \mathbf{E}_{\text{base}}^{(l)}, \quad l = 1, 2, \dots, s \quad (6)$$

where $\mathbf{E}_{\text{base}}^{(l)}$ represents the original DUST3R decoder features. This produces global low-resolution point maps $\{\mathbf{X}_k\}_{k=1}^N$ while preserving the enhanced intermediate decoder features $\{\hat{\mathbf{E}}_{\text{scene}}^{(l)}\}_{l=1}^s$ for potential refinement when humans appear small in the scene.

3.3 Human-Centric Refinement

When humans occupy small pixel regions in input images, we activate a refinement module to address resolution limitations and boundary inaccuracies from the global processing.

This refinement enables precise depth and geometry estimation for human-centric regions by leveraging both global scene context and local geometric details.

3.3.1 Input Cropping and Preparation

We begin by extracting bounding boxes from the SMPL depth maps to crop human regions from the input images $\{\mathbf{I}_k^{\text{crop}}\}_{k=1}^N$, monocular depth maps, and global point clouds $\{\mathbf{X}_k^{\text{crop}}\}_{k=1}^N$. $\mathbf{X}_k^{\text{crop}}$ are then upsampled via bicubic interpolation to match the resolution of the cropped image regions, providing dense spatial $\hat{\mathbf{F}}_{\text{point}}$. In parallel, we preserve multi-scale decoder features $\{\hat{\mathbf{F}}_{\text{scene}}^{(l)}\}_{l=2}^s$ from the global processing, which encode valuable scene context for cross-module integration.

The cropped images and monocular depth maps are processed through the same encoder and Feature Fusion Module as in global processing, generating multi-level crop-specific features $\{\hat{\mathbf{F}}_{\text{crop}}^{(l)}\}_{l=1}^s$ enriched with high-frequency local geometry.

3.3.2 Cross-Module Decoder Integration

To effectively combine global and local information, the refinement decoder incorporates cross-attention at each decoding layer. The integration process follows a two-step approach:

Initial Layer Integration: At the first decoder layer ($l = 1$), we integrate spatial guidance from upsampled point clouds:

$$\hat{\mathbf{E}}_{\text{crop}}^{(1)} = \text{ZeroConv}(\hat{\mathbf{F}}_{\text{crop}}^{(1)}) + \text{ZeroConv}(\hat{\mathbf{F}}_{\text{point}}) + \hat{\mathbf{E}}_{\text{crop base}}^{(1)} \quad (7)$$

Cross-Module Attention: For subsequent layers ($l = 2, \dots, s$), we apply cross-attention between local crop features and preserved global scene context:

$$\hat{\mathbf{F}}_{\text{crop}}^{(l)} = \text{CrossAttn}(\hat{\mathbf{F}}_{\text{crop}}^{(l)}, \hat{\mathbf{F}}_{\text{scene}}^{(l)}) \quad (8)$$

$$\hat{\mathbf{E}}_{\text{crop}}^{(l)} = \text{ZeroConv}(\hat{\mathbf{F}}_{\text{crop}}^{(l)}) + \hat{\mathbf{E}}_{\text{crop base}}^{(l)} \quad (9)$$

where $\hat{\mathbf{F}}_{\text{crop}}^{(l)}$ provides human features from the cropped pointmap region, $\hat{\mathbf{F}}_{\text{scene}}^{(l)}$ introduces global context preserved from scene processing, $\hat{\mathbf{F}}_{\text{point}}$ represents spatial guidance from upsampled point clouds, and $\hat{\mathbf{E}}_{\text{crop base}}^{(l)}$ denotes the intermediate hidden representations from the refinement decoder itself. This formulation ensures that the decoder remains aware of both fine-scale human shapes and the global scene layout.

Output Integration. The refinement decoder produces high-resolution point maps for each cropped region. Thanks to the use of spatial guidance and consistent camera intrinsics, the output is inherently aligned with the global coordinate system. We resize the refined point maps back to

the original resolution and integrate them into the global point clouds through spatial alignment in the image domain. This design enables high-fidelity human reconstruction while maintaining geometric consistency between human regions and the surrounding scene.

3.4. Fine-tuning on Human Dynamic Videos

Both global processing and human-centric refinement use the same fine-tuning loss following DUST3R:

$$L_{dust3r} = \mathbf{C}_v^e \left\| \frac{1}{z} \mathbf{X}_v^e - \frac{1}{\bar{z}} \bar{\mathbf{X}}_v^e \right\|_2 - \alpha \log \mathbf{C}_v^e \quad (10)$$

where $v \in \{n, m\}$ denotes the view index, \mathbf{X} and $\bar{\mathbf{X}}$ are the predicted and ground-truth point maps, \mathbf{C}_v^e is the correspondence confidence map, z and \bar{z} are scaling factors used to normalize the predicted and ground truth point maps, and α is the same hyperparameter as in DUST3R. Notably, global processing and refinement use the same z and \bar{z} for consistency.

4. Experiment

4.1. Experimental Setting

Training datasets. For fine-tuning, we use two synthetic datasets and one real-world dataset. The synthetic datasets are Bedlam [3] and GTA-IM [8], while the real dataset is BEHAVE [2]. All datasets are downsampled to 5 FPS.

Training details. Our Human3R is initialized with the weight of Align3R [33] and trained using AdamW [32] with a learning rate of 5×10^{-5} and a batch size of 5 on 7 NVIDIA H800 GPUs. Training our model on 5×10^4 pairs for 50 epochs in each of main pipeline and refinement separately takes approximately one week in total.

4.2. Video Depth Estimation

Evaluating dataset. For evaluation, we use five datasets, comprising three real-world datasets—Bonn [35], TUM Dynamics [38], and BEHAVE [2], and two synthetic datasets, GTA-IM and Bedlam. For GTA-IM and Bedlam, we ensure that the evaluation scenes and human motions are entirely distinct from those used in the training set. For BEHAVE, we use the designated evaluation subset of the dataset. For Bonn [35] and TUM Dynamics [38], we select three scenes featuring human subjects.

Evaluation metrics. For quantitative evaluation, we mainly report two widely used depth metrics: absolute relative error (Abs Rel) and the percentage of inlier points (with a threshold value of $\delta < 1.25$). Furthermore, we follow the evaluation protocol established by MonST3R [51] to ensure a fair comparison with existing methods.

Baselines. We compare our Human3R with 1 diffusion-based 4D feed forward reconstruction method: **Geo4D** [23], and three non-diffusion-based methods: **MonST3R** [51], **Align3R** [33], and **VGGT** [41].

Results. Table 1 presents the quantitative results for video depth estimation. Our Human3R demonstrates superior performance on real-world datasets, achieving the best results on BEHAVE (Abs Rel: 0.033, $\delta < 1.25$: 0.992), Bonn (Abs Rel: 0.077), and TUM Dynamics (Abs Rel: 0.102, $\delta < 1.25$: 0.907). On synthetic datasets, our method shows competitive performance on GTA-IM (second-best Abs Rel: 0.112, best $\delta < 1.25$: 0.869), while Geo4D performs better on Bedlam due to its diffusion-based nature. Overall, our approach effectively handles human-centric scenes with complex interactions.

4.3. Camera Pose Estimation

Evaluating dataset. For evaluation, we use three datasets, comprising two real-world datasets—Bonn, TUM Dynamics—and one synthetic dataset, GTA-IM.

Evaluation metrics. We follow the evaluation protocol from previous works [33] and report three metrics: Absolute Trajectory Error (ATE), Relative Translation Error (RTE), and Relative Rotation Error (RRE). ATE measures the absolute difference between estimated and ground truth camera trajectories. RTE and RRE measure the relative translation and rotation errors between consecutive frames, respectively.

Results. Table 2 shows the camera pose estimation results. Our Human3R achieves the best performance on synthetic GTA-IM dataset across all metrics (ATE: 0.015, RTE: 0.010, RRE: 0.227), demonstrating significant improvements in temporal consistency and geometric coherence for human-centric scenes. On real-world datasets, our method shows competitive performance, achieving second-best ATE on TUM Dynamics (0.335) and second-best RTE on Bonn (0.285), while obtaining the best RRE on TUM Dynamics (0.430).

4.4. Ablation Study

4.4.1 Prior Incorporation

To validate the effectiveness of our Feature Fusion Module (FFM) in incorporating SMPL priors, we conduct a controlled ablation study on a representative sequence from the GTA dataset. We compare three model variants: our proposed FFM, a baseline without SMPL prior incorporation (only mono prior), and a naive fusion approach without FFM.

Experimental Setup. We train all models on 1,000 image pairs from the same GTA sequence for 50 epochs under

Category	Method	Synthetic				Real-World			
		GTA-IM		Bedlam		BEHAVE		Bonn 3 scenes	
		Abs Rel \downarrow $\delta < 1.25 \uparrow$							
Diffusion based	Geo4D [23]	0.218	0.717	0.058	0.943	0.194	0.752	0.087	0.966
	MonST3R [51]	0.265	0.626	0.115	0.884	0.082	0.903	0.094	0.915
	Align3R [33]	0.138	0.775	<u>0.086</u>	<u>0.935</u>	<u>0.049</u>	<u>0.966</u>	<u>0.086</u>	0.938
	Non-Diffusion VGGT [41]	0.104	<u>0.807</u>	0.200	0.646	0.699	0.904	0.267	0.943
	Ours	0.112	0.869	0.107	0.855	0.033	0.992	0.077	0.959
									0.102
									0.907

Table 1. **Video depth estimation results.** We evaluate our model on both real-world datasets: Bonn and TUM dynamics, Behave, and synthetic datasets: GTA-IM, and Bedlam. For Bonn and TUM dynamics we just pick scenes with human. **Best** and second best results are highlighted.

Category	Method	GTA-IM			Bonn 3 scenes			TUM dynamics		
		ATE \downarrow	RTE \downarrow	RRE \downarrow	ATE(10^{-2}) \downarrow	RTE(10^{-2}) \downarrow	RRE \downarrow	ATE(10^{-2}) \downarrow	RTE(10^{-2}) \downarrow	RRE \downarrow
Diffusion based	Geo4D [23]	0.107	0.222	5.66	0.367	0.321	0.282	0.461	<u>0.269</u>	0.480
	MonST3R [51]	0.039	0.160	<u>3.23</u>	0.499	0.276	0.521	0.407	0.271	0.506
	Align3R [33]	0.036	0.120	6.28	0.519	0.298	0.510	0.295	0.240	0.432
	Non-Diffusion VGGT [41]	0.292	0.292	8.69	<u>0.460</u>	0.544	0.535	0.337	0.294	0.591
	Ours	0.015	0.010	0.227	0.473	<u>0.285</u>	<u>0.503</u>	<u>0.335</u>	0.290	0.430

Table 2. **Camera pose estimation results.** We evaluate our model on two real-world datasets: TUM dynamics and Bonn, as well as the synthetic dataset: GTA-IM. **Best** and second best results are highlighted.

identical training conditions. We evaluate three configurations:

- **Only mono:** Uses only monocular depth features without any SMPL prior incorporation.
- **w/o FFM:** Incorporates SMPL priors through simple linear addition:

$$\hat{\mathbf{E}}_{\text{scene}}^{(l)} = \text{ZeroConv}(\hat{\mathbf{F}}_{\text{mono}}^{(l)}) + \text{ZeroConv}(\hat{\mathbf{F}}_{\text{smpl}}^{(l)}) + \mathbf{E}_{\text{base}}^{(l)} \quad (11)$$

- **w. FFM:** Our full model employing the multi-head attention-based gating mechanism described in Section 3 to intelligently fuse multi-modal features.

Results. As shown in Table 3, incorporating SMPL priors significantly improves depth estimation performance. Comparing "only mono" with our fusion approaches, we observe substantial improvements: Absolute Relative error drops from 0.054 to 0.034 (37% improvement), and accuracy within the 1.25 threshold increases from 0.978 to 0.980.

More importantly, our Feature Fusion Module demonstrates clear advantages over naive fusion. The FFM achieves better Absolute Relative error (0.034 vs 0.036) and higher accuracy (0.980 vs 0.978) compared to simple linear addition. While Log RMSE shows mixed results, with "only mono" achieving the best score (0.125), this metric can be sensitive to outliers and doesn't reflect the overall improvement in depth quality.

Qualitative Analysis. Our qualitative evaluation demonstrates progressive improvements across different fusion strategies. The naive linear addition approach (w/o FFM) introduces artifacts in background regions where SMPL priors are irrelevant, leading to degraded depth estimation quality in non-human areas. This occurs because simple fusion can-

Setting	Abs Rel \downarrow $\delta < 1.25 \uparrow$	Log RMSE \downarrow
only mono	0.042	0.978
w/o FFM	<u>0.037</u>	0.978
w. FFM	0.035	0.980

Table 3. **Ablation study on Feature Fusion Module (FFM).**

not distinguish between regions where human body priors are beneficial versus regions where they introduce noise.

Unlike simple linear addition, our gating mechanism learns to selectively incorporate SMPL depth information when it provides reliable geometric constraints while down-weighting it in regions where image-based features are more reliable. This adaptive fusion strategy prevents potential conflicts between different modalities and enables more robust depth estimation across the entire scene. Additional qualitative Figure ref comparisons are provided in the supplementary material.

The results demonstrate that: (1) SMPL prior incorporation is essential for accurate human depth estimation; (2) naive fusion can introduce artifacts; and (3) our FFM provides the most effective integration strategy. The superior performance of FFM can be attributed to its ability to adaptively weight the contribution of human body priors based on scene context. Unlike simple linear addition, which treats all features equally, our gating mechanism learns to selectively incorporate SMPL depth information when it provides reliable geometric constraints while down-weighting it in regions where image-based features are more reliable.

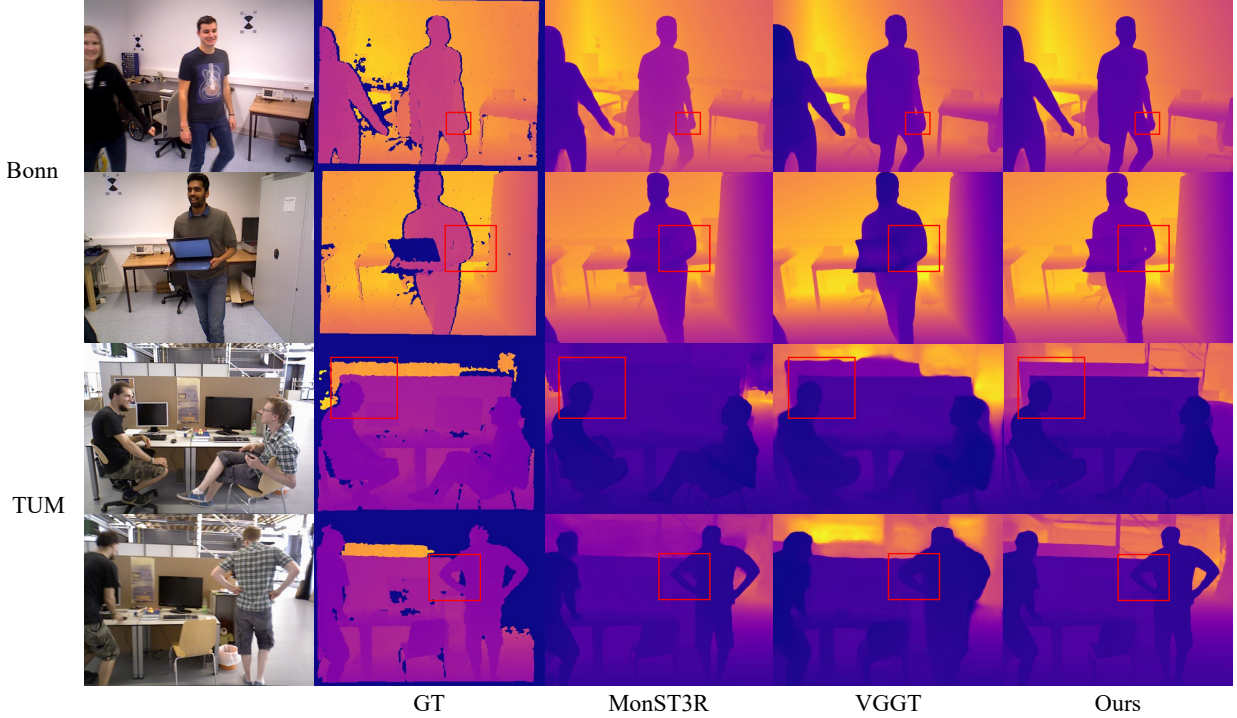


Figure 3. Qualitative Comparison on Bonn and Tum dynamic Datasets. The red boxes highlight the comparison regions, demonstrating that our method outperforms existing works.

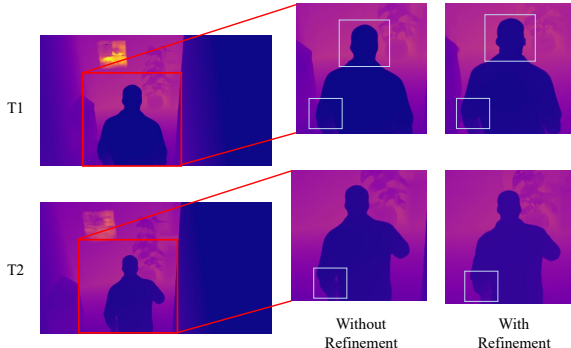


Figure 4. Qualitative comparison of human reconstruction on Human3R with and without refinement. Our refinement module produces more accurate human geometry and maintains better temporal consistency across frames in the cropped human regions.

4.4.2 Refinement

To validate the effectiveness of our refinement strategy in improving human reconstruction quality and temporal stability, we conduct qualitative comparisons on human-centric regions. Figure 4 demonstrates the visual improvements achieved through our hierarchical refinement approach.

Qualitative Analysis. As shown in Figure 4, our refinement strategy yields significant improvements in human

reconstruction quality. The refined results exhibit sharper anatomical details and more accurate geometric boundaries compared to the base model without refinement. More importantly, the refinement module enhances temporal consistency across video sequences, reducing flickering artifacts and maintaining stable human geometry throughout dynamic movements.

The improvements are particularly evident in challenging scenarios involving complex human poses and occlusions. Our hierarchical pipeline, which processes full-resolution images for overall scene geometry while applying strategic cropping and cross-attention fusion for human-specific detail enhancement, successfully preserves fine-grained human boundaries while maintaining global scene consistency. This demonstrates that our refinement approach effectively addresses the anatomical inconsistencies and boundary degradation issues commonly observed in existing methods.

5. Conclusion

We proposed Human3R, a novel approach for monocular dynamic video reconstruction in human-centric scenes that addresses anatomical artifacts and resolution degradation issues. Our method incorporates hybrid geometric priors combining SMPL human body models with monocular depth estimation for anatomically plausible reconstruction.

The hierarchical pipeline processes full-resolution images for scene geometry while applying strategic cropping and cross-attention fusion for human detail enhancement. Experiments on TUM Dynamics and GTA-IM datasets validate superior performance in resolving anatomical inconsistencies and boundary degradation.

References

- [1] Shariq Farooq Bhat, Reiner Birk, Diana Wofk, Peter Wonka, and Matthias Müller. Zoedepth: Zero-shot transfer by combining relative and metric depth, 2023. [3](#)
- [2] Bharat Lal Bhatnagar, Xianghui Xie, Ilya Petrov, Cristian Sminchisescu, Christian Theobalt, and Gerard Pons-Moll. Behave: Dataset and method for tracking human object interactions. In *IEEE Conference on Computer Vision and Pattern Recognition (CVPR)*. IEEE, 2022. [6](#)
- [3] Michael J. Black, Priyanka Patel, Joachim Tesch, and Jinlong Yang. BEDLAM: A synthetic dataset of bodies exhibiting detailed lifelike animated motion. In *Proceedings IEEE/CVF Conf. on Computer Vision and Pattern Recognition (CVPR)*, pages 8726–8737, 2023. [6](#)
- [4] Aleksei Bochkovskii, Amaël Delaunoy, Hugo Germain, Marcel Santos, Yichao Zhou, Stephan R. Richter, and Vladlen Koltun. Depth pro: Sharp monocular metric depth in less than a second, 2025. [3](#)
- [5] Yohann Cabon, Lucas Stoffl, Leonid Antsfeld, Gabriela Csurka, Boris Chidlovskii, Jerome Revaud, and Vincent Leroy. Must3r: Multi-view network for stereo 3d reconstruction, 2025. [2](#)
- [6] Zhongang Cai, Daxuan Ren, Ailing Zeng, Zhengyu Lin, Tao Yu, Wenjia Wang, Xiangyu Fan, Yang Gao, Yifan Yu, Liang Pan, Fangzhou Hong, Mingyuan Zhang, Chen Change Loy, Lei Yang, and Ziwei Liu. HuMMAn: Multi-modal 4d human dataset for versatile sensing and modeling. In *17th European Conference on Computer Vision, Tel Aviv, Israel, October 23–27, 2022, Proceedings, Part VII*, pages 557–577. Springer, 2022. [3](#)
- [7] Yukang Cao, Jiahao Lu, Zhisheng Huang, Zhuowen Shen, Chengfeng Zhao, Fangzhou Hong, Zhaoxi Chen, Xin Li, Wenping Wang, Yuan Liu, et al. Reconstructing 4d spatial intelligence: A survey. *arXiv preprint arXiv:2507.21045*, 2025. [2, 3](#)
- [8] Zhe Cao, Hang Gao, Karttikeya Mangalam, Qizhi Cai, Minh Vo, and Jitendra Malik. Long-term human motion prediction with scene context. In *ECCV*. 2020. [6, 2](#)
- [9] Weirong Chen, Ganlin Zhang, Felix Wimbauer, Rui Wang, Nikita Araslanov, Andrea Vedaldi, and Daniel Cremers. Back on track: Bundle adjustment for dynamic scene reconstruction, 2025. [3](#)
- [10] Xingyu Chen, Yue Chen, Yuliang Xiu, Andreas Geiger, and Anpei Chen. Easi3r: Estimating disentangled motion from dust3r without training, 2025. [2, 3](#)
- [11] Seokju Cho, Jiahui Huang, Seungryong Kim, and Joon-Young Lee. Seurat: From moving points to depth, 2025. [3](#)
- [12] Kai Deng, Zexin Ti, Jiawei Xu, Jian Yang, and Jin Xie. Vggt-long: Chunk it, loop it, align it – pushing vggt’s limits on kilometer-scale long rgb sequences, 2025. [3](#)
- [13] Sai Kumar Dwivedi, Yu Sun, Priyanka Patel, Yao Feng, and Michael J. Black. Tokenhmr: Advancing human mesh recovery with a tokenized pose representation, 2024. [4](#)
- [14] Sven Elflein, Qunjie Zhou, and Laura Leal-Taixé. Light3r-sfm: Towards feed-forward structure-from-motion. In *Proceedings of the IEEE/CVF Conference on Computer Vision and Pattern Recognition (CVPR)*, pages 16774–16784, 2025. [2](#)
- [15] Shariq Farooq Bhat, Ibraheem Alhashim, and Peter Wonka. Adabins: Depth estimation using adaptive bins. In *2021 IEEE/CVF Conference on Computer Vision and Pattern Recognition (CVPR)*, page 4008–4017. IEEE, 2021. [3](#)
- [16] Haiwen Feng, Junyi Zhang, Qianqian Wang, Yufei Ye, Pengcheng Yu, Michael J. Black, Trevor Darrell, and Angjoo Kanazawa. St4rtrack: Simultaneous 4d reconstruction and tracking in the world, 2025. [3](#)
- [17] Bulat Gabdullin, Nina Konovalova, Nikolay Patakin, Dmitry Senushkin, and Anton Konushin. Depthart: Monocular depth estimation as autoregressive refinement task, 2025. [3](#)
- [18] Stefano Gasperini, Nils Morbitzer, HyunJun Jung, Nassir Navab, and Federico Tombari. Robust monocular depth estimation under challenging conditions. In *2023 IEEE/CVF International Conference on Computer Vision (ICCV)*. IEEE, 2023. [3](#)
- [19] Shubham Goel, Georgios Pavlakos, Jathushan Rajasegaran, Angjoo Kanazawa, and Jitendra Malik. Humans in 4d: Reconstructing and tracking humans with transformers, 2023. [4](#)
- [20] Jisang Han, Honggyu An, Jaewoo Jung, Takuya Narihira, Junyoung Seo, Kazumi Fukuda, Chaehyun Kim, Sunghwan Hong, Yuki Mitsuji, and Seungryong Kim. d^2ust3r : Enhancing 3d reconstruction with 4d pointmaps for dynamic scenes, 2025. [3](#)
- [21] Jiahui Huang, Qunjie Zhou, Hesam Rabeti, Aleksandr Kordova, Huan Ling, Xuanchi Ren, Tianchang Shen, Jun Gao, Dmitry Slepichev, Chen-Hsuan Lin, Jiawei Ren, Kevin Xie, Joydeep Biswas, Laura Leal-Taixé, and Sanja Fidler. Vipe: Video pose engine for 3d geometric perception. In *NVIDIA Research Whitepapers*, 2025. [3](#)
- [22] Wonbong Jang, Philippe Weinzaepfel, Vincent Leroy, Lourdes Agapito, and Jerome Revaud. Pow3r: Empowering unconstrained 3d reconstruction with camera and scene priors, 2025. [2](#)
- [23] Zeren Jiang, Chuanxia Zheng, Iro Laina, Diane Larlus, and Andrea Vedaldi. Geo4d: Leveraging video generators for geometric 4d scene reconstruction, 2025. [3, 6, 7](#)
- [24] Angjoo Kanazawa, Michael J. Black, David W. Jacobs, and Jitendra Malik. End-to-end recovery of human shape and pose, 2018. [4](#)
- [25] Nikos Kolotouros, Georgios Pavlakos, Michael J. Black, and Kostas Daniilidis. Learning to reconstruct 3d human pose and shape via model-fitting in the loop, 2019. [4](#)
- [26] Samuel Li, Pujith Kachana, Prajwal Chidananda, Saurabh Nair, Yasutaka Furukawa, and Matthew Brown. Rig3r: Rig-aware conditioning for learned 3d reconstruction, 2025. [3](#)

[27] Wenyu Li, Sidun Liu, Peng Qiao, and Yong Dou. Mono3r: Exploiting monocular cues for geometric 3d reconstruction, 2025. 2

[28] Zhengqi Li, Richard Tucker, Forrester Cole, Qianqian Wang, Linyi Jin, Vickie Ye, Angjoo Kanazawa, Aleksander Holynski, and Noah Snavely. Megasam: Accurate, fast, and robust structure and motion from casual dynamic videos, 2024. 3

[29] Yiqing Liang, Abhishek Badki, Hang Su, James Tompkin, and Orazio Gallo. Zero-shot monocular scene flow estimation in the wild, 2025. 3

[30] Chenguo Lin, Yuchen Lin, Panwang Pan, Yifan Yu, Honglei Yan, Katerina Fragkiadaki, and Yadong Mu. Movies: Motion-aware 4d dynamic view synthesis in one second, 2025. 3

[31] Sidun Liu, Wenyu Li, Peng Qiao, and Yong Dou. Regist3r: Incremental registration with stereo foundation model, 2025. 2

[32] Ilya Loshchilov and Frank Hutter. Decoupled weight decay regularization. In *International Conference on Learning Representations*, 2017. 6

[33] Jiahao Lu, Tianyu Huang, Peng Li, Zhiyang Dou, Cheng Lin, Zhiming Cui, Zhen Dong, Sai-Kit Yeung, Wenping Wang, and Yuan Liu. Align3r: Aligned monocular depth estimation for dynamic videos, 2024. 2, 3, 6, 7

[34] Dominic Maggio, Hyungtae Lim, and Luca Carlone. Vggt-slam: Dense rgb slam optimized on the sl(4) manifold, 2025. 2

[35] Emanuele Palazzolo, Jens Behley, Philipp Lottes, Philippe Giguère, and Cyrill Stachniss. Refusion: 3d reconstruction in dynamic environments for rgb-d cameras exploiting residuals. In *2019 IEEE/RSJ International Conference on Intelligent Robots and Systems (IROS)*, page 7855–7862. IEEE Press, 2019. 6, 3

[36] Priyanka Patel and Michael J. Black. Camerahmr: Aligning people with perspective, 2024. 4

[37] René Ranftl, Alexey Bochkovskiy, and Vladlen Koltun. Vision transformers for dense prediction, 2021. 3

[38] J. Sturm, N. Engelhard, F. Endres, W. Burgard, and D. Cremers. A benchmark for the evaluation of rgb-d slam systems. In *Proc. of the International Conference on Intelligent Robot Systems (IROS)*, 2012. 6

[39] Zhenggang Tang, Yuchen Fan, Dilin Wang, Hongyu Xu, Rakesh Ranjan, Alexander Schwing, and Zhicheng Yan. Mvdust3r+: Single-stage scene reconstruction from sparse views in 2 seconds, 2024. 2

[40] Hengyi Wang and Lourdes Agapito. 3d reconstruction with spatial memory, 2024. 2

[41] Jianyuan Wang, Minghao Chen, Nikita Karaev, Andrea Vedaldi, Christian Rupprecht, and David Novotny. Vggt: Visual geometry grounded transformer, 2025. 2, 3, 6, 7

[42] Qianqian Wang, Yifei Zhang, Aleksander Holynski, Alexei A. Efros, and Angjoo Kanazawa. Continuous 3d perception model with persistent state, 2025. 3

[43] Shuzhe Wang, Vincent Leroy, Yohann Cabon, Boris Chidlovskii, and Jerome Revaud. Dust3r: Geometric 3d vision made easy. In *Proceedings of the IEEE/CVF Conference on Computer Vision and Pattern Recognition*, pages 20697–20709, 2024. 2

[44] Yifan Wang, Jianjun Zhou, Haoyi Zhu, Wenzheng Chang, Yang Zhou, Zizun Li, Junyi Chen, Jiangmiao Pang, Chunhua Shen, and Tong He. π^3 : Scalable permutation-equivariant visual geometry learning, 2025. 3

[45] Yuxi Xiao, Jianyuan Wang, Nan Xue, Nikita Karaev, Yuri Makarov, Bingyi Kang, Xing Zhu, Hujun Bao, Yujun Shen, and Xiaowei Zhou. Spatialtrackerv2: 3d point tracking made easy, 2025. 3

[46] Tian-Xing Xu, Xiangjun Gao, Wenbo Hu, Xiaoyu Li, Song-Hai Zhang, and Ying Shan. Geometrycrafter: Consistent geometry estimation for open-world videos with diffusion priors, 2025. 3

[47] Lihe Yang, Bingyi Kang, Zilong Huang, Xiaogang Xu, Jiashi Feng, and Hengshuang Zhao. Depth anything: Unleashing the power of large-scale unlabeled data, 2024. 3

[48] David Yifan Yao, Albert J. Zhai, and Shenlong Wang. Uni4d: Unifying visual foundation models for 4d modeling from a single video, 2025. 3

[49] Ye Yuan, Umar Iqbal, Pavlo Molchanov, Kris Kitani, and Jan Kautz. Glamr: Global occlusion-aware human mesh recovery with dynamic cameras, 2022. 4

[50] Bowei Zhang, Lei Ke, Adam W. Harley, and Katerina Fragkiadaki. Tapip3d: Tracking any point in persistent 3d geometry, 2025. 3

[51] Junyi Zhang, Charles Herrmann, Junhwa Hur, Varun Jampani, Trevor Darrell, Forrester Cole, Deqing Sun, and Ming-Hsuan Yang. Monst3r: A simple approach for estimating geometry in the presence of motion, 2025. 2, 3, 6, 7

[52] Songyan Zhang, Yongtao Ge, Jinyuan Tian, Guangkai Xu, Hao Chen, Chen Lv, and Chunhua Shen. Pomato: Marrying pointmap matching with temporal motion for dynamic 3d reconstruction, 2025. 3

Human3R: Incorporating Human Priors for Better 3D Dynamic Reconstruction from Monocular Videos

Supplementary Material

6. More Feature Fusion Module Details

In our pipeline, We employ two separate feature fusion modules for image 1 and image 2, each structured as illustrated in Figure 5. The cross-attention mechanism within each module utilizes 8 attention heads.

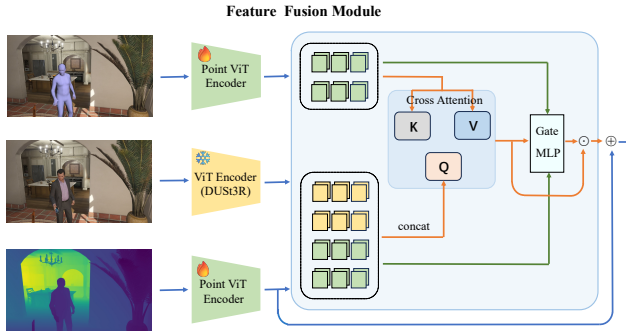


Figure 5. Detail of Feature Fusion Module.

7. More Ablation Study Results

7.1. Qualitative Analysis of Prior Incorporation

Figure 6 provides detailed qualitative comparisons of our Feature Fusion Module (FFM) against baseline approaches. The results demonstrate the progressive improvements achieved through our multi-modal fusion strategy.

7.2. Depth Alignment Ablation Study

To validate the necessity of aligning monocular and SMPL depth maps as described in Section 3.2.1, we conduct an ablation study comparing our RANSAC-based alignment approach with direct fusion of unaligned depths.

Experimental Setup. We compare two configurations on the same GTA sequence used in our FFM ablation study:

- **w/o Alignment:** Directly incorporates raw monocular depth \hat{D}_k^{Mono} and SMPL depth \hat{D}_k^{SMPL} into the Feature Fusion Module without any scale or offset correction.
- **w. Alignment:** Our full approach using RANSAC-based linear transformation (Equations 1-2) to obtain aligned depth $\hat{D}_k^{\text{Aligned}}$ before feature extraction and fusion.

Results and Analysis. As shown in Table 4, the absence of depth alignment severely degrades performance. Without proper alignment, significant scale and offset discrepancies between monocular and SMPL depth estimates create conflicting geometric signals during training. This leads to several critical issues:

Setting	Abs Rel \downarrow	$\delta < 1.25 \uparrow$	Log RMSE \downarrow
w/o Align	5.12	0.084	1.834
w. Align	0.035	0.980	0.137

Table 4. Ablation study on Depth AlignmentM).

- **Prior rejection:** The network learns to treat SMPL depth as noise rather than meaningful geometric constraints, with the Feature Fusion Module suppressing rather than selectively incorporating SMPL features.
- **Cross-attention failure:** Scale inconsistencies prevent the multi-head attention mechanism from establishing meaningful correspondences between depth modalities.
- **Training instability:** Conflicting depth representations hinder effective multi-modal learning, resulting in substantially worse performance across all metrics.

The dramatic performance difference (Abs Rel: 5.12 vs 0.035) demonstrates that our RANSAC-based alignment is not merely a preprocessing convenience, but a fundamental requirement for effective multi-modal fusion. By ensuring consistent depth representation across estimation sources, the alignment step enables the network to properly utilize SMPL priors as complementary geometric information, validating the critical importance of this component in our pipeline.

8. More Qualitative Results

8.1. Camera pose comparison

Figure 7 demonstrates the camera pose estimation performance of our Human3R method compared to existing approaches on the GTA-IM dataset. Our method achieves superior trajectory accuracy and temporal consistency, particularly in human-centric scenes.

8.2. Dynamic point clouds

Figure 8 shows the 3D point cloud reconstructions on real-world datasets. Our approach produces more complete and geometrically consistent point clouds, especially in human body regions where SMPL priors provide valuable geometric constraints. The results demonstrate the effectiveness of our multi-modal fusion strategy in preserving both human body structure and background scene geometry.

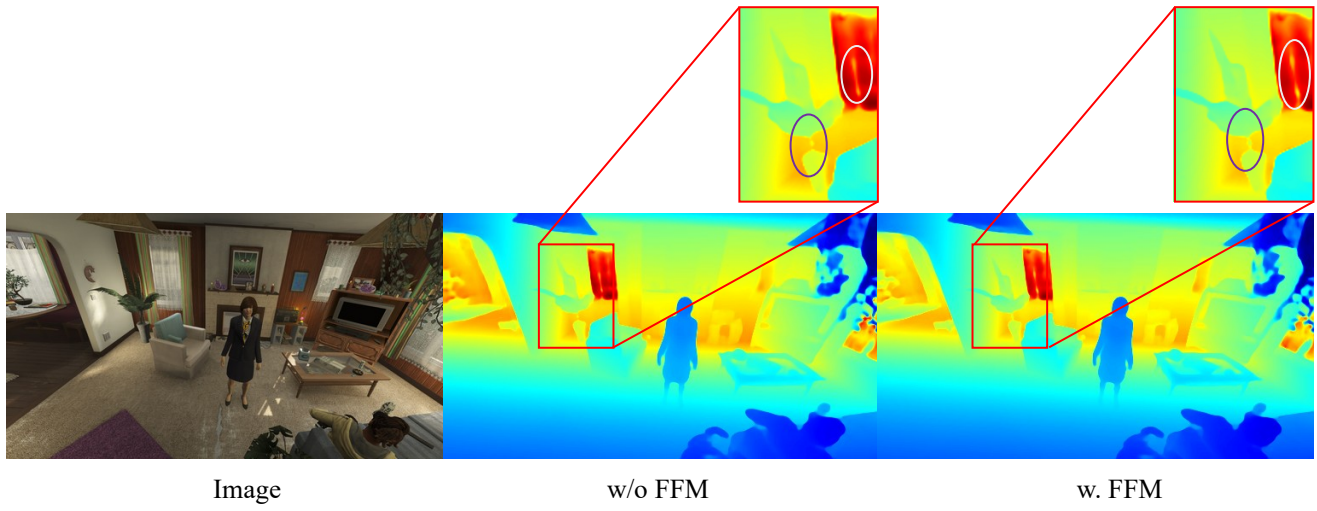


Figure 6. Qualitative ablation study on Prior Incorporation. The naive fusion approach (w/o FFM) introduces artifacts in background regions where SMPL priors are irrelevant, while our FFM preserves background quality.

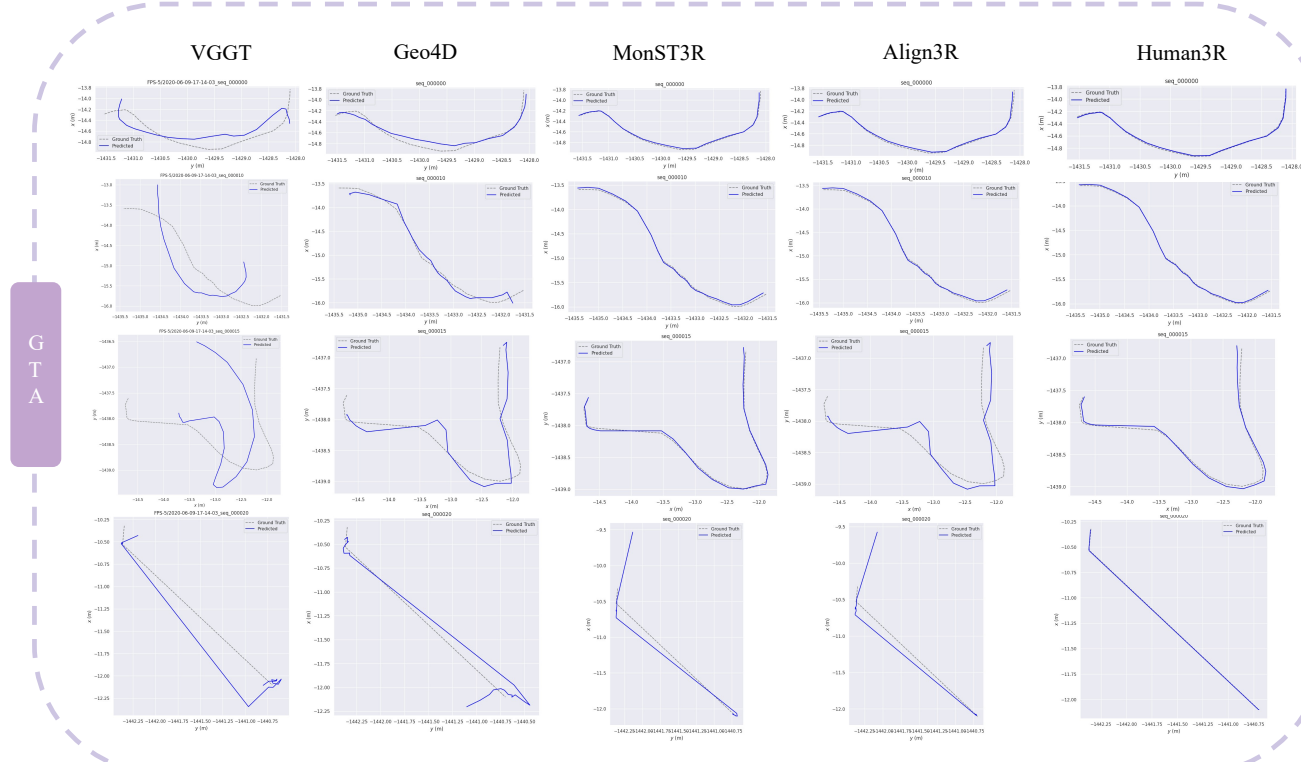


Figure 7. Camera pose estimation comparison on the GTA-IM[8] with existing work

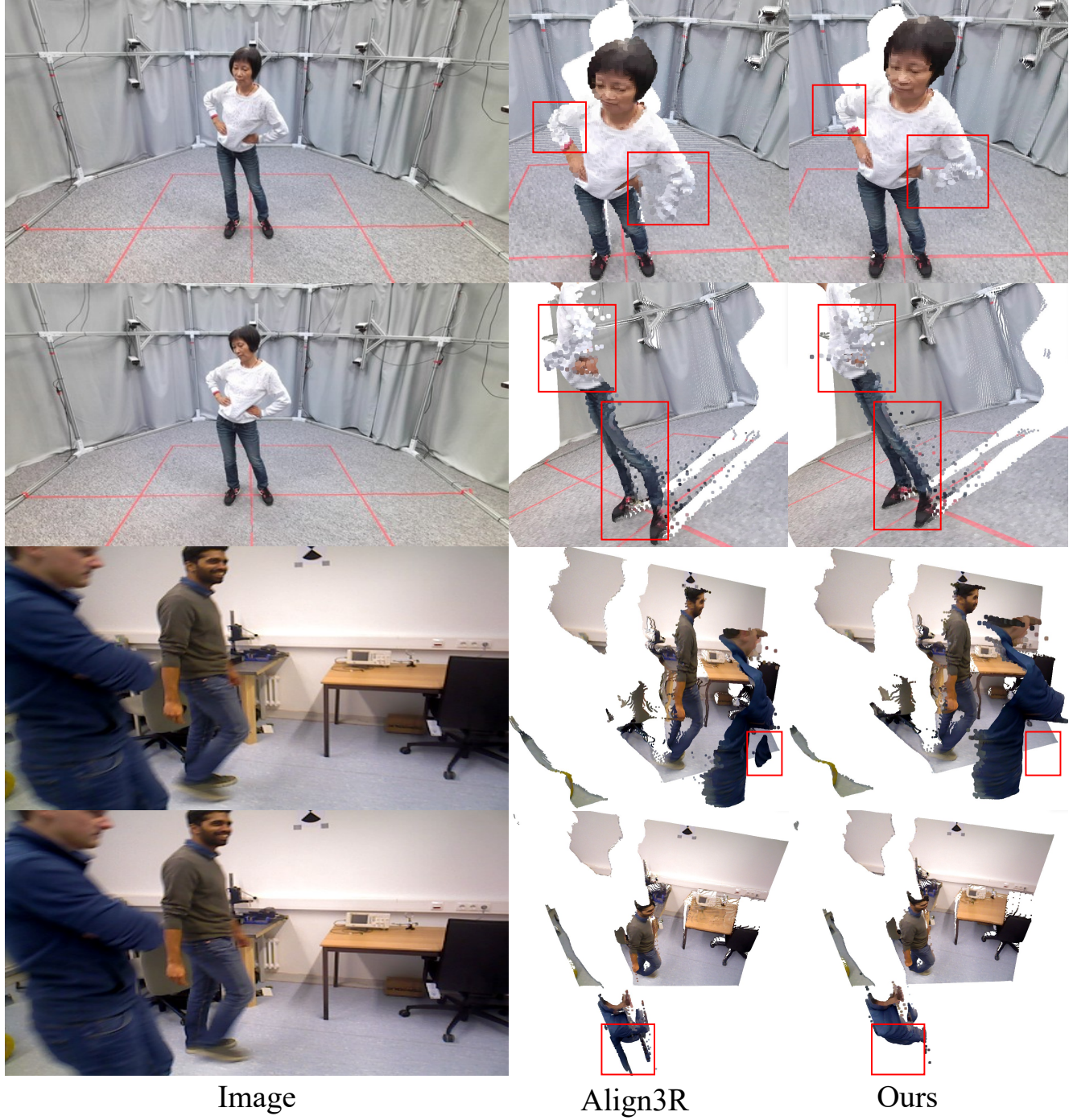


Figure 8. Visualization of point clouds on the HuMMan [6] and Bonn [35]. The visualizations highlight regions (marked in red boxes) where our approach produces more accurate and detailed human reconstructions compared to Align3R.